Vertical SNS weak-link Josephson junction fabricated from only boron-doped diamond

M. Watanabe,[1] R. Kanomata,[1] S. Kurihara,[1] A. Kawano,[1] S. Kitagoh,[1] T. Yamaguchi,[2] Y. Takano,[2] and H. Kawarada[1,*]

[1]*School of Science and Engineering, Waseda University, 3-4-1 Okubo, Shinjyuku-ku, Tokyo 169-8555, Japan*

[2]*National Institute for Materials Science, 1-2-1 Sengen, Tsukuba, Ibaraki 305-0047, Japan*

(Received 5 December 2010; revised manuscript received 10 February 2012; published 14 May 2012)

A vertical superconductor/normal conductor/superconductor (SNS) weak-link Josephson junction has been successfully fabricated from only homoepitaxial diamond films. Superconducting diamond, normal-state diamond, and superconducting diamond are homoepitaxially grown in a sequence. The temperature dependence of the critical superconducting current was fitted using Likharev's theory of SNS weak-link junctions. When the normal-state-diamond thickness L is much larger than the coherent length in the normal-state-diamond ξ_n, an exponential temperature dependence of normalized critical current was observed, indicating a proximity effect. Shapiro steps in the current-voltage characteristics under microwave irradiation were observed in the junction with $L \gg \xi_n$.

DOI: 10.1103/PhysRevB.85.184516 PACS number(s): 74.45.+c, 74.70.Wz, 85.25.Cp, 71.30.+h

I. INTRODUCTION

Diamond is a well-known insulator with a band gap of 5.5 eV; however, its electrical conductivity can be controlled up to 10^3 S/cm by doping boron as an acceptor. Boron has one less electron than carbon; thus, boron doping introduces hole carriers into a diamond valence band. The electronic structure of boron-doped diamond is well described by the rigid band model, and the impurity level of boron is 0.37 eV above the valence band maximum. With increasing boron concentration, diamond starts to exhibits metallic conduction. Since the discovery of superconductivity in heavily boron-doped diamond,[1] the relationship between boron concentration in diamond and superconducting (SC) properties has been studied in various forms of diamond such as polycrystalline and single-crystalline diamond[2–4] and so on. An insulator-to-metal transition (IMT) occurs at a boron concentration of approximately 3×10^{20} cm^{-3}.[4–8] Metallic diamond exhibits superconductivity at a low temperature induced by the strong phonon interaction. A heavily boron-doped diamond film with a boron concentration of $N_B = 8 \times 10^{21}$ cm^{-3} has an SC transition temperature (T_c) of approximately 9 K.[3,9–12] Diamond is a unique material in that it can behave as an insulator, semiconductor, metal, and superconductor by simply tuning the boron concentration, suggesting the possibility of forming a Josephson junction with SC and normal-conducting (NC) layers composed of only diamond films.

In this study, we have fabricated a vertical SC/NC/SC (SNS) weak-link Josephson junction using only homoepitaxial diamond following the procedure outlined in Ref. 12. The fabrication of a Josephson junction using homoepitaxial diamond is ideal since the junction between the superconducting and nonsuperconducting regions maintains seamless properties without a barrier to electric conduction. Shapiro steps indicate that an alternating current Josephson effect was observed for our Josephson junction.

II. FABRICATION OF VERTICAL SNS WEAK-LINK JOSEPHSON JUNCTION

The Josephson junction with a vertical SNS structure, in which NC diamond film is sandwiched between SC diamond films, fabricated using only diamond, is shown in Fig. 1. Type-Ib high-pressure, high-temperature (HPHT) single-crystal diamond was used for the substrate. All diamond films were homoepitaxially deposited on the substrate by microwave plasma-enhanced chemical vapor deposition (MPCVD). Diamond deposition was carried out using CH_4 at a concentration of 1–3% diluted with hydrogen, a pressure during growth of 80 Torr, and a growth temperature of 840–900 °C. For the growth of the superconducting films, trimethylboron ($B[CH_3]_3$) was used as a dopant gas. A high B/C ratio of 6000 ppm was chosen for the deposition of superconducting diamond films, whereas the boron-containing gas was intentionally not used to deposit nonsuperconducting diamond film. To form a vertical Josephson junction, a selective epitaxial growth technique was applied to fabricate a stacked structure[12] and contact layers as shown in Fig. 1.

Using plasma-assisted chemical vapor deposition, the stacking of the layers of the Josephson junction was performed by the sequential homoepitaxial growth of diamond layers with boron as a dopant. To obtain a flat and uniform surface initially, a heavily boron-doped diamond film was homoepitaxially grown by MPCVD on a single-crystal HPHT synthetic diamond substrate as the lower SC layer. The first homoepitaxial growth with boron concentration of 6×10^{21} cm^{-3} was carried out selectively using a gold mask. After removing the mask, two boron-doped diamond films, one with NC layer of 1–2 $\times 10^{20}$ cm^{-3} and one acting as the upper SC layer with a boron concentration of 6×10^{21} cm^{-3}, were sequentially deposited.[12] Note that the boron concentration of the NC film was lower than the critical concentration for the IMT of 3×10^{20} cm^{-3}.[2–4] The area of the junction where the upper SC layer and NC layer overlapped with the lower SC layer was 5000 μm^2 (50 μm $\times$ 100 μm). Using a focused ion beam (FIB), the junction area was reduced to 5 μm^2 (1 μm $\times$ 5 μm).

III. RESULTS AND DISCUSSION

The depth profile of the boron concentration for the fabricated SNS Josephson junction was obtained by secondary ion mass spectroscopy (SIMS). Figure 2 shows the boron concentrations of the upper SC layer, NC layer, and lower

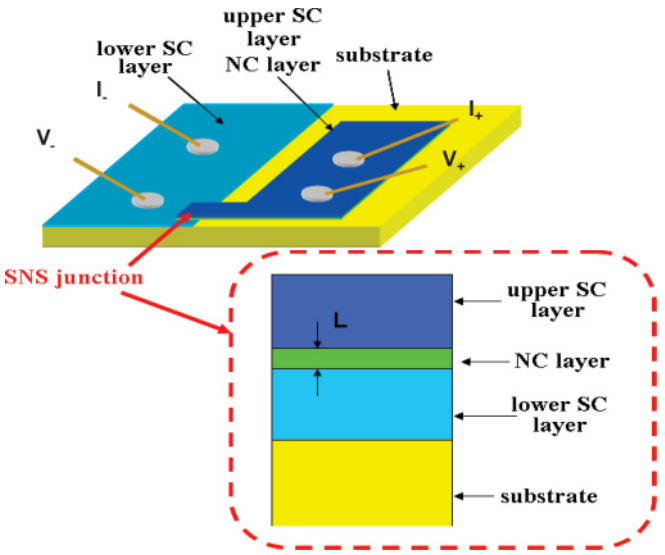

FIG. 1. (Color online) Schematic of SNS junction and cross section of the junction. The Josephson junction was a vertical SNS structure, in which a normal-state diamond film (NC layer) was sandwiched between two superconducting diamond films (lower SC layer and upper SC layer). On an HPHT synthetic type-Ib (111) diamond substrate, the lower SC layer, the NC layer, and the upper NC layer are sequentially homoepitaxially grown. The boron concentrations of the two SC layers were approximately the same.

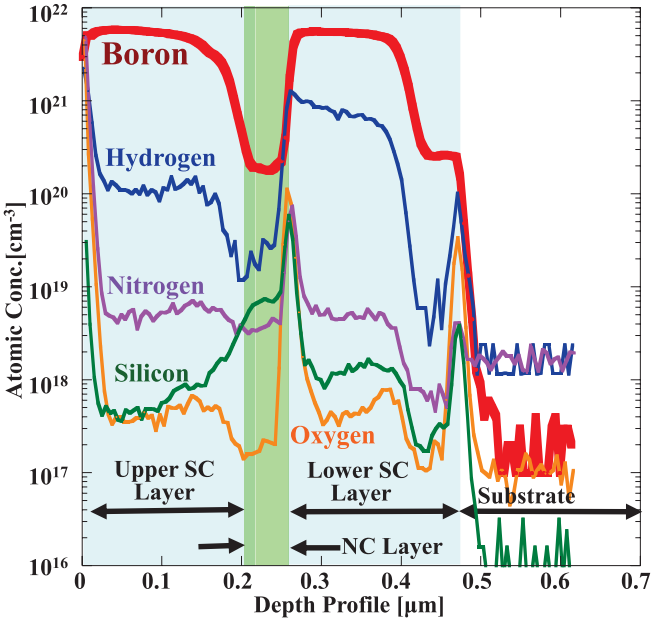

FIG. 2. (Color) Depth profiles of the junction obtained by SIMS. The lower SC layer is heavily boron doped with a boron concentration and thickness of 6×10^{21} cm^{-3} and 173 nm, respectively. The NC layer has a low boron concentration of 1–2 $\times$ 10^{20} cm^{-3} and a thickness of 40 nm. The boron concentration is lower than that at which the insulator-metal transition occurs (3×10^{20} cm^{-3}). The upper SC layer is heavily boron doped with a boron concentration and thickness of 6×10^{21} cm^{-3} and 210 nm, respectively.

SC layer, which were estimated to be 6×10^{21} cm^{-3}, 1–2 $\times$ 10^{20} cm^{-3}, and 6×10^{21} cm^{-3}, respectively. The thickness of the NC layer (L) was found to be approximately 50 nm, in which the boron concentration was abruptly reduced to slightly below the IMT concentration (3×10^{20} cm^{-3}) since the boron source gas was not supplied during its deposition. From the depth profile obtained by SIMS, the vertical SNS junction was verified to consist of a very thin NC layer sandwiched between SC layers.

A cross-sectional transmission electron microscope (TEM) image of this junction is shown in Fig. 3. The bright-field image was observed to be homogeneous, indicating that the junction area was single-crystal, which was also verified by a selected area diffraction (SAD) pattern. Crystal defects such as dislocations were observed, but there were no microtwins. The dashed lines in the image represent the interfaces between the SC layer and NC layer, which correspond to the distribution of boron concentration measured by SIMS shown in Fig. 2. The dislocation shown at the center of the TEM image might start at the interface between the substrate and the lower SC layer. However, this interface was not observed clearly. There is only a faint contrast at the interface between the lower SC layer and the NC layer, because after the lower SC layer was grown, the sample surface was subjected to a photolithography process to form a metal mask for the selective epitaxial growth for the upper SC layer. These results suggest that the homoepitaxial growth of highly boron-doped diamond by plasma-assisted CVD was nearly perfect.

The temperature dependence of the resistance of the as-deposited junction is shown in Fig. 4. The overlapping area between the upper SC and the lower SC was 5000 μm^2 (50 μm $\times$ 100 μm). T_c for this junction was 4.5 K. The resistance decreased rapidly at approximately 9 K, but it did not decrease to zero. The resistance gradually decreased as the temperature was further decreased, reaching zero resistance at 4.5 K. The inset shows the temperature dependence of the resistance for the lower and upper SC layers; a very sharp superconducting transition was observed. The values of T_c for the lower and upper SC layers were estimated to be 7.9 K and 8.8 K, respectively. This difference in T_c is due to differences in crystallinity or carrier density.

Figure 5 shows the $I-V$ characteristics of the junction at 2 K. The junction area had already been reduced to 5 μm^2 by an FIB. Constant currents were supplied from I_+ to I_-, and the

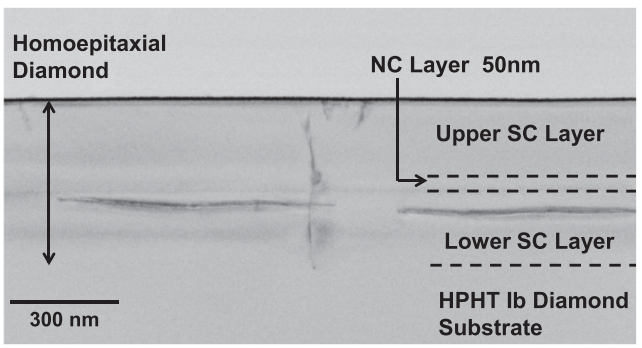

FIG. 3. Cross-sectional transmission electron microscope image of the Josephson junction. This junction was composed of homoepitaxial single-crystalline diamond, though there were a few crystal defects.

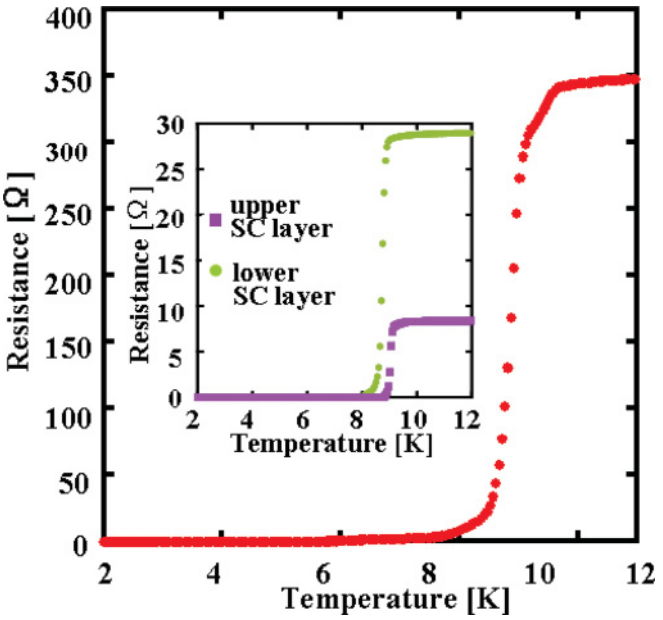

FIG. 4. (Color online) Temperature dependence of the resistance of the as-deposited junction before its size was reduced using an FIB system. T_c for this junction was 4.5 K. The resistance decreased rapidly at approximately 9 K, but did not decrease to zero. The inset shows the temperature dependence of the resistance for the lower and upper SC layers. The values of T_c for the lower and upper SC layers were estimated to be 7.9 K and 8.8 K, respectively.

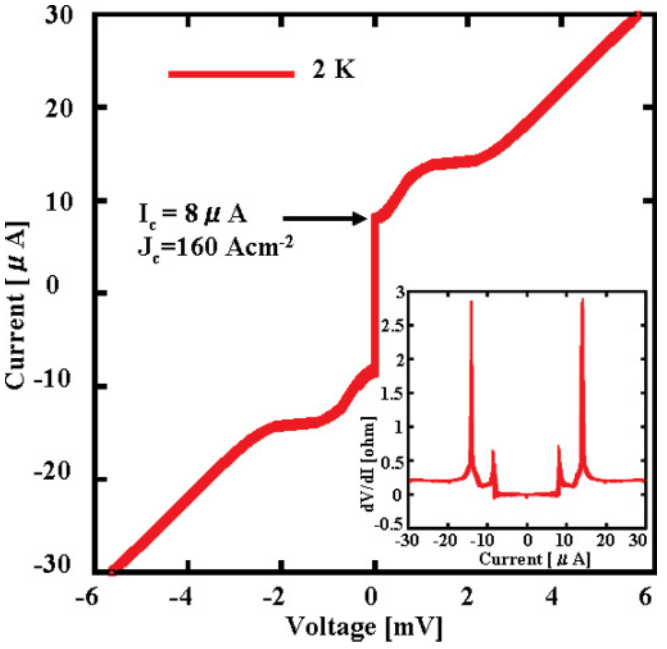

FIG. 5. (Color online) $I-V$ characteristics of the junction at 2 K. The junction area is 5 um^2. I_c is 8 μA, and J_c was estimated to be 160 A cm^{-2}. The inset shows the (dI/dV)-V characteristics of this $I-V$ curve. An increase in resistance occurred twice. It is likely that I_c was different for the upper and lower SC layers.

corresponding voltage drop between V_+ and V_- was measured. The current due to the penetration from the SC layers was measured at 0 V as critical current. The critical current I_c was 8 μA, and the critical current density J_c was estimated to be 160 A cm^{-2}, which is three orders of magnitude smaller than that of the bulk crystal measured to be $J_c = 240{,}000$ A cm^{-2} in a 4.8×10^{-2} μm^2 structure. The shape of this $I-V$ curve was slightly unusual compared with that for a typical Josephson junction. The inset of Fig. 5 shows (dI/dV)-V characteristic of this $I-V$ curve. The resistance drops steeply at currents of 14 μA and 8 μA. Features such as the one at 14 μA might be caused by spurious circuit elements (capacitances, inductances) connected to the Josephson junction. The shape of the $I-V$ curve between -11 μA and 11 μA was very close to that for a well-known resistively shunted junction (RSJ) model.

The $I-V$ characteristics of the junction at 2 K under microwave irradiation are shown in Figs. 6(a) and (b). Seven steps ($n = 2$–8) with an interval of 2.1×10^{-5} V were induced by the irradiation of microwaves with a frequency of 10 GHz and an irradiation power of -10.5 dBm [Fig. 6(a)]. The steps are certified by dI/dV oscillations. Upon the irradiation of 15 GHz microwaves, at least two steps ($n = 2$ and 4) were observed at an irradiation power of -14 dBm with an interval of 3.1×10^{-5} V, which is also apparent by dI/dV [Fig. 6(b)]. The microwave frequencies and voltage intervals show good agreement with the theoretical formula for the Josephson effect.

$$V_n = \frac{nh}{2e}\nu_0 \quad (\mathrm{n} = \mp 1,\ \mp 2, \ldots) \tag{1}$$

Here, V_n is the interval between the steps, h is Planck's constant, and ν_0 is the frequency of the irradiated microwaves. The obtained Shapiro steps in the vertical SNS junctions are of poor quality caused by the shunt path at the side wall of the junction. The path might be located at the partially graphitized side wall after FIB treatment to reduce the size of the junction and is not caused by the homoepitaxial growth. Despite the low quality, the steps are good evidence for the AC Josephson effect.

Our NC layer made of boron-doped diamond is a highly doped semiconductor with a boron concentration of 2×10^{20} cm^{-3}, where the hole mean free path l_n is much lower than the coherent length ξ_n, the values of which reflect the mean size of a Cooper pair in a normal-conducting material. At the dirty limit ($l_n \ll \xi_n$), ξ_n can be written[13] by expanding de Gennes' proximity theory[14,15] to a three-dimensional free-electron gas model as follows:

$$\xi_n = (\hbar^3 \mu / 6\pi k_B T e m^*)^{1/2} (3\pi^2 n)^{1/3} \tag{2}$$

where m^* is the effective mass of the carriers, μ is the carrier mobility, and n is the carrier density of the semiconductor. This expression has been successfully applied to estimate ξ_n for an SNS Josephson junction with a Pb/highly B-doped Si/Pb structure,[16] where the N region is highly boron-doped Si. The SNS structure is analogous to that of highly boron-doped diamond. Here, if we assume $m^* = 0.4 \times 9.1 \times 10^{-31}$ and $\mu = 2$ cm^2/Vsec, then ξ_n of the diamond NC layer ($n = 1.7 \times 10^{20}$ cm^{-3}) is estimated to be 3 nm from Eq. (2).

The temperature dependence as seen on Fig. 7 for the critical superconducting current $I_c(T;L)$ of the Josephson junction was measured in the range $0.4\ T_c < T < T_c$ for the sample for which characteristics are shown in Figs. 2–6. The

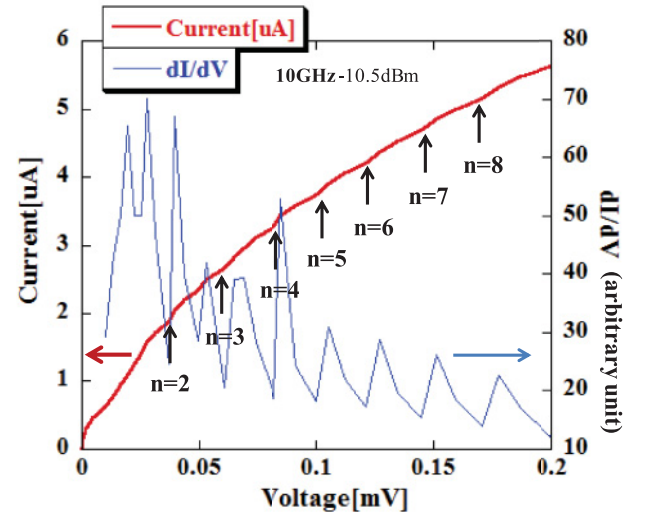

(a)

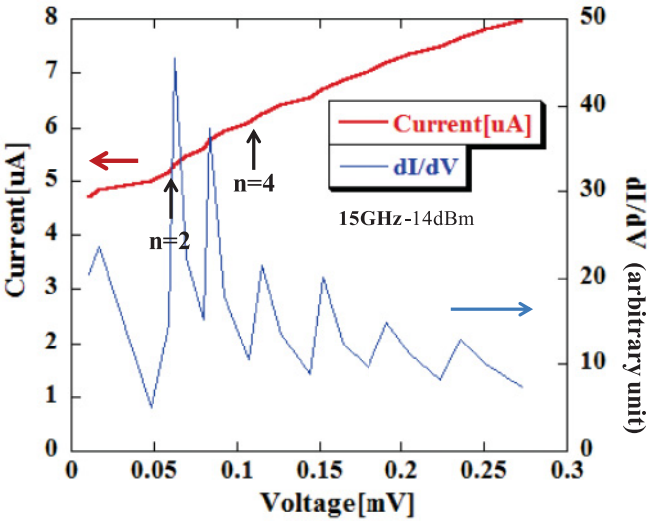

(b)

FIG. 6. (Color online) $I-V$ characteristics under microwave irradiation. (a) Irradiation at a frequency of 10 GHz and an irradiation power of -10.5 dBm. Seven steps ($n = 2$–8) with an interval of 2.1×10^{-5} V can be observed. These steps are certified by dI/dV oscillations. (b) Irradiation at a frequency of 15 GHz and irradiation power of -14 dBm. The interval between steps is 3.1×10^{-5} V, which is certified by the dI/dV curve. The irradiation frequencies and voltage intervals fit the theoretical formula for the Josephson effect.

values shown in Fig. 7 were normalized by the currents at $0.4T_c$ ($I_c[T;L]/I_c[0.4T_c;L]$). The experimental plots are well fitted by the rigid-boundary SNS theory (solid line) developed by Likharev and Kupriyanov[17,18] and Zubkov and Kupriyanov,[19] as given below.

$$I_c(T;L) = \frac{2}{\pi e R_n}\frac{|\Delta_\infty|^2}{kT_c}\frac{L/\xi_n}{\sinh(L/\xi_n)} \quad (0.3T_c < T < T_c)$$
$$\cong \frac{4}{\pi e R_n}\frac{|\Delta_\infty|^2}{kT_c}\frac{L}{\xi_n}e^{-L/\xi_n} \qquad (3)$$

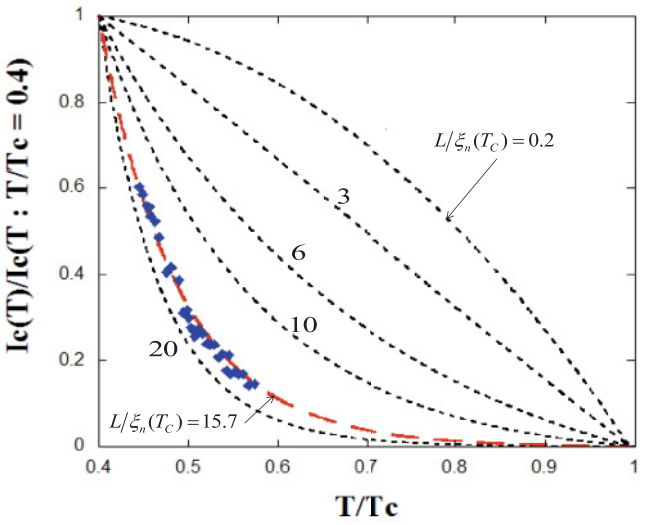

FIG. 7. (Color) The temperature dependence of the critical superconducting current I_c normalized by current at $0.4T_c$ and I_c for $L/\xi_n(T_c) = 3$–20 calculated from Likharev's theory of SNS junctions in the dirty limit. The fitted $L_{\text{eff}}/\xi_n(T_c)$ for our sample was 15.7.

where R_n is the normal-state zero-bias resistance of the junction, Δ_∞ is the superconducting gap in the bulk of the superconductor (from the gap equation in BCS theory), L is the distance between the electrodes (the thickness of the NC layer), and ξ_n is the coherent length in the normal conductor. Δ_∞ was calculated self-consistently by the following equation:

$$\Delta_\infty = N(0)V\int_0^{\hbar\omega_D}\left\{\Delta_\infty \times \tanh\left[\frac{1}{2}\beta\left(\xi^2+\Delta_\infty^2\right)^{1/2}\right]\Big/\left(\xi^2+\Delta_\infty^2\right)^{1/2}\right\}d\xi \qquad (4)$$

where ω_D is Debye frequency, and β is $1/k_B$. Typically, the dependence of I_c on L for junctions with $L \gg \xi_n(T)$ is fitted to the dependence $\exp(-L/\xi_n[\mathrm{T}])$ [see Eq. (3)]. $L/\xi_n(T)$ is an important parameter in determining the temperature dependence of I_c properties.[20,21] The dependence of the normalized I_c on the reduced temperature calculated for $L/\xi_n(T) = 3$–20 is shown in Fig. 7. The signature of the proximity effect in SNS junctions is the exponential-like behavior of $\exp(-L_{\text{eff}}/\xi_n)$,[21] which was calculated for the present structures with a large $L/\xi_n(T_c)$ of 3–20 as shown in Fig. 7. The critical current temperature dependence was good agreement with the theoretical value at $L/\xi_n(T_c) = 15.7$, with the assumption of $L = 50$ nm estimated from Figs. 2 and 3. The exponential fitting is evidence of the proximity effect observed at a weak link. A typical example of the proximity effect is clearly visible in the experimental data obtained for low-T_c SNS junctions in the early work on Pb–Cu–Pb sandwich junctions by Clarke[22] and microbridge junctions.[23] Similar phenomena were observed in semiconductors such as Te, Si, and InAs acting as an interlayer in SNS devices.[13,16,24] In the semiconductor NC layer, the discontinuity at the interface is unavoidable due to a Schottky barrier or a large mismatch in Fermi wavevectors between the SC and NC layers, which is unavoidable.[21] Although the coherent length of semiconductor diamond is less than that of other semiconductors, the

continuity at the interface provides a barrier-free penetration for the Fermi wave, resulting in a proximity effect over a relatively long distance (∼50 nm). The proximity effect in a homogeneous junction has been achieved for the first time using a homoepitaxial diamond sandwich structure.

IV. CONCLUSION

A vertical SNS weak-link Josephson junction has been fabricated from only boron-doped diamond layers by controlling the doping concentration. The temperature dependence of the critical superconducting current was fitted to Likharev's theory of SNS weak-link junctions. When the nonsuperconducting layer thickness L is more than 10 times longer than the coherent length $\xi_n(T_c)$, the normalized critical current density exhibits exponential-like behavior, $\exp(-L_{\mathrm{eff}}/\xi_n)$, indicating the proximity effect in the SNS structure. A Josephson junction made of homogeneous SNS materials without a discontinuity at the interface in junctions will be further studied using highly boron-doped diamonds.

ACKNOWLEDGMENTS

This research was partially supported by a Grant-in-Aid for Scientific Research S (No.19106006) from the Ministry of Education, Culture, Sports, Science and Technology, Japan, and by the Advanced Low Carbon Technology and Research Development Program (ALCA) of the Japan Science and Technology Agency.

*kawarada@waseda.jp

[1] E. A. Ekimov, V. A. Sidorov, E. D. Bauer, N. N. Mel'nik, N. J. Curro, J. D. Thompson, and S. M. Stishov, Nature **428**, 542 (2004).
[2] E. Bustarret, J. Kačmarčik, C. Marcenat, E. Gheeraert, C. Cytermann, J. Marcus, and T. Klein, Phys. Rev. Lett. **93**, 237005 (2004).
[3] Y. Takano, M. Nagao, I. Sakaguchi, M. Tachiki, T. Hatano, H. K. Kobayashi, H. Umezawa, and H. Kawarada, Appl. Phys. Lett. **85**, 2851 (2004).
[4] A. Kawano, H. Ishiwata, S. Iriyama, R. Okada, T. Yamaguchi, Y. Takano, and H. Kawarada, Phys. Rev. B **82**, 085318 (2010).
[5] H. Umezawa, T. Takenouchi, K. Kobayashi, Y. Takano, M. Nagao, M. Tachiki, T. Hatano, and H. Kawarada, New Diam. Front. Carbon Technol. **17**, 1 (2007).
[6] T. Yokoya, T. Nakamura, T. Matsushita, T. Muro, Y. Takano, M. Nagao, T. Takenouchi, H. Kawarada, and T. Oguchi, Nature **438**, 647 (2005).
[7] Y. Takano, M. Nagao, T. Takenouchi, H. Umezawa, I. Sakaguchi, M. Tachiki, and H. Kawarada, Diamond Relat. Mater. **14**, 1936 (2005).
[8] A. Kawano, H. Ishiwata, S. Iriyama, R. Okada, S. Kitagoh, M. Watanabe, Y. Takano, T. Yamaguchi, and H. Kawarada, Physica C **470**, S604 (2010).
[9] Y. Takano, J. Phys.: Condens. Matter **21**, 253201 (2009).
[10] H. Umezawa, T. Takenouchi, Y. Takano, K. Kobayashi, M. Nagao, I. Sakaguchi, M. Tachiki, T. Hatano, G. Zhong, M. Tachiki, and H. Kawarada, e-print arXiv:cond-mat/0503303 (2005).
[11] Y. Takano, T. Takenouchi, S. Ishii, S. Ueda, T. Okutsu, I. Sakaguchi, H. Umezawa, H. Kawarada, and M. Tachiki, Diamond Relat. Mater. **16**, 911 (2007).
[12] M. Watanabe, A. Kawano, S. Kitagoh, T. Yamaguchi, Y. Takano, and H. Kawarada, Physica C **470**, S613 (2010).
[13] J. Seto and T. Van Duzer, in *Low-Temperature Physics, LT-13*, edited by W. J. O'Sullivan, K. D. Timmerhaus, and E. F. Hammel (Plenum, New York, 1972), Vol. 3, p. 328.
[14] P. G. de Gennes, Rev. Mod. Phys. **36**, 225 (1964).
[15] P. G. de Gennes, *Superconductivity of Metals and Alloys* (Benjamin, New York, 1969).
[16] T. Nishino, E. Yamada, and U. Kawabe, Phys. Rev. B **33**, 2042 (1986).
[17] K. K. Likharev, Rev. Mod. Phys. **51**, 101 (1979).
[18] M. Yu. Kupriyanov and V. F. Likharev, Sov. J. Low. Temp. Phys. **8**, 562 (1982) [Fiz. Nizk. Temp. **8**, 1045 (1982)].
[19] A. A. Zubkov and M. Yu. Kupriyanov, Sov. J. Low. Temp. Phys. **9**, 279 (1983) [Fiz. Nizk. Temp. 548 (1983)].
[20] K. A. Deline and T. P. Orlando, *Foundations of Applied Superconductivity* (Addison-Wesley, New York, 1991), p. 558.
[21] K. A. Deline and A. W. Kleinsasser, Supercond. Sci. Technol. **9**, 227 (1996).
[22] J. Clarke, Proc. R. Soc. A **308**, 447 (1969).
[23] J. M. Warlaumont, J. C. Brown, and R. A. Buhrman, Appl. Phys. Lett. **34**, 415 (1979).
[24] H. Takayanagi and T. Kawakami, Phys. Rev. Lett. **54**, 2449 (1985).